APL Materials

Soft peripheral nerve interface made from carbon nanotubes embedded in silicone

Cite as: APL Mater. **8**, 101111 (2020); https://doi.org/10.1063/5.0021887
Submitted: 15 July 2020 . Accepted: 06 October 2020 . Published Online: 20 October 2020

Korkut Terkan, Francisco Zurita, Touba Jamal Khalaf, Philipp Rinklin, Tetsuhiko Teshima, Tobias Kohl, and Bernhard Wolfrum

Soft peripheral nerve interface made from carbon nanotubes embedded in silicone

Cite as: APL Mater. 8, 101111 (2020); doi: 10.1063/5.0021887
Submitted: 15 July 2020 • Accepted: 6 October 2020 •
Published Online: 20 October 2020

Korkut Terkan,[1] Francisco Zurita,[1] Touba Jamal Khalaf,[1] Philipp Rinklin,[1] Tetsuhiko Teshima,[1,2] Tobias Kohl,[3] and Bernhard Wolfrum[1,4,a)]

AFFILIATIONS

[1]Neuroelectronics, Munich School of Bioengineering, Department of Electrical and Computer Engineering, Technical University of Munich, Boltzmannstrasse 11, 85748 Garching, Germany
[2]Medical & Health Informatics Laboratories, NTT Research Incorporated, 1950 University Ave. Suite 600 East Palo Alto, California 94303, USA
[3]Chair of Zoology, Technical University of Munich, Liesel-Beckmann-Strasse 4, 85354 Freising Weihenstephan, Germany
[4]Institute of Biological Information Processing, Bioelectronics (IBI-3), Forschungszentrum Jülich, 52425 Jülich, Germany

Note: This paper is part of the Special Topic on Advances in Bioelectronics.
[a)]**Author to whom correspondence should be addressed:** bernhard.wolfrum@tum.de

ABSTRACT

Electrodes for interfacing implantable electronics and neural tissue are of great importance to gain a better understanding of the nervous system and to help people suffering from impaired body functions due to nerve lesions or lost organ functionality. In particular, neurostimulation techniques for bioelectronic medicine rely on the development of mechanically and electrochemically stable electrodes. While contemporary electrodes are based mainly on metals, new materials are being designed to enhance the mechanical and electrochemical properties of the interface. In this work, a nerve interface based on carbon nanotubes (CNTs) embedded in polydimethylsiloxane (PDMS) is fabricated and investigated. The fabrication process relies on the selective vacuum filtration of CNT suspensions through a printed wax pattern. The mechanical and electrochemical stability of the nerve interface was validated by 10 000 stretching cycles up to 20% strain and >4 × 10^6 biphasic stimulation pulses with 32 μC cm^{-2} per phase. The feedline resistance and electrode impedance showed only minor alterations after the stress tests. The functionality of the nerve interface was demonstrated by successful stimulation of the central nerve cord of a horse leech applying stimulation conditions within the water window of the CNT/PDMS electrodes. This work shows the practical usability of CNT/PDMS composites as electrodes and feedlines in peripheral nerve interfaces for future neuroprosthetic devices.

INTRODUCTION

Electrical stimulation of nerve and muscle tissue is a powerful tool for treating neurological disorders,[1] restoring impaired functionality,[2] and providing insight into understanding information processing in the nervous system.[3] In this context, electrodes in direct contact or in close proximity to the target tissue are used as transceivers between the biologic and the electronic signal processing domains.

Contemporary materials for stimulation electrodes are mainly based on metals such as stainless steel,[4] platinum,[5] platinum–iridium,[6] nickel–titanium,[7] and other alloys. Often, the surface of metal electrodes is modified by inducing porosity[8] and oxide formation[9] or coating with carbon nanotubes (CNTs) and conducting polymers like poly(3,4-ethylenedioxythiophene).[10] These surface alterations have the purpose to modify the electrochemical properties of bare metal electrodes in order to achieve a lower impedance and higher charge injection capacity (CIC). Consequently, higher currents can be injected into the tissue through the electrode without reaching potentials at the electrode–electrolyte interface that might cause damage to the tissue or the electrodes by irreversible electrochemical reactions.[11,12]

Although metals are the dominant material used for commercial implantable electrodes, they pose certain limitations. For example, when current pulses are applied at the electrodes for longer periods of time, metal dissolution for stainless steel and platinum[13,14]

was observed. This issue can have toxic effects on the neural tissue.[15]

Besides the aspects of desired electrochemical properties and stability of the electrodes, the substrate of the implanted device should have similar mechanical properties as the tissue to which it is in contact. Soft and flexible interfaces conform better to neural tissue[16] and elicit less neural damage during relative movements inside the body. In particular, such soft interfaces initiate less foreign body response compared to more rigid ones when implanted.[17] This aspect is of special importance as an inflammatory response can lead to fibrous capsule formation around the electrode, which in turn decreases the signal-to-noise ratio for recording devices or induces higher current thresholds to reach the target tissue when stimulating. Two main routes of providing flexible neural interfaces are currently being employed: One is based on the fabrication on extremely thin substrate films made, for example, from polyimide[18,19] or parylene.[20,21] The second approach employs soft and stretchable substrates made of, e.g., silicones such as polydimethylsiloxane (PDMS).[22–24] While the integration of metallic feedlines on flexible substrates is not a problem in general, it turns out to be a challenge on soft and stretchable substrates due to the potential electrical connection breakage upon strain application. However, it was reported that by structuring the electrical connections in a meandering fashion,[25] patterning intrinsically stretchable polymeric composites,[26] or making use of microcracks in thin metal films,[27] elastomeric substrates can be stretched up to tens of percent while still sustaining sufficient electrical conductivity. Another approach to realize soft and stretchable neural interfaces is embedding high-aspect ratio nanomaterials, e.g., gold-coated titanium oxide nanowires, inside the PDMS matrix.[28] As another nanomaterial with a high-aspect ratio, CNTs have been successfully embedded in PDMS.[29–33] Typically, electrodes made out of CNTs exhibit a large specific surface area and, therefore, a high specific double layer capacitance when used in contact with electrolyte solutions.[34] This property enables CNT electrodes to store more charge[11,35] making them a promising candidate for stimulation electrodes. Furthermore, CNTs have a larger water window than metals[5,36,37] and consequently can be polarized to higher potentials without electrolysis of water. This is important since irreversible electrochemical reactions due to Faradaic currents during electrolysis can damage the tissue or the electrode.

Here, we present a soft and stretchable neural interface device with CNTs as the sole conducting material inside a PDMS matrix. The CNT/PDMS electrodes were structured using a printed wax pattern on a filter membrane, as introduced by Tybrandt and Vörös for the fabrication of silver nanowire feedlines.[38] We present the electrochemical and mechanical properties of the CNT/PDMS electrodes and validate the device's functionality by extracellular stimulation inside a horse leech (*Haemopis sanguisuga*). The stimulation is performed between two adjacent ganglia on its main ventral nerve cord, and its muscle contraction is correlated with the applied stimulation signals.

MATERIALS AND METHODS

Fabrication

Filter membranes (Durapore, 0.22 μm pore size, polyvinylidene fluoride (PVDF) membrane, ∅ 47 mm, hydrophilic, nonsterile) were patterned with the negative structure of the desired electrode layout by a wax printer (Xerox, ColorQube 8900). Afterward, they were wetted with de-ionized (DI) water from both sides and attached to a vacuum filtration setup. A CNT dispersion was prepared with 1.43 mg CNTs (Hanos MWCNT M-95, entangled, 93%–97% purity; Hanwha Chemical), 16 mg sodium dodecyl sulfate (SDS) (BioChemica, A2573.0250, pH = 5.0–7.0), and 100 ml DI water. The CNT amount was defined by the area of the target electrode design to yield a surface concentration of 1.33 mg cm^{-2} after filtration. An ultrasonic homogenizer (generator: GM 2200.2, transducer: UW 2200, booster: SH213, sonotrode: KE76, Bandelin, Germany) was used at 40% power for 5 min continuously to disperse the CNTs in the solvent. Subsequently, the dispersion was filtered through the patterned filter membrane to achieve a homogeneous CNT pattern on the wax-free areas of the membrane. The vacuum for the filtration was applied by a pump (MD 1, 1.5 mbar, Vacuubrand GmbH+CoKG, Germany). The membranes were left to dry for at least 16 h. Afterward, they were dipped into acetone four times with breaks of 5 min in between each step. This step removed the wax pattern and residual CNTs, which were not captured in the defined areas but adhered to the wax pattern. Before the next step, the membrane was left to dry for at least one hour. Meanwhile, a glass slide was cleaned with isopropanol and dried with pressurized air. PDMS (Sylgard 184) was prepared by vigorously stirring a 10:1 (w:w) base to curing agent mixture for 2 min and degassing it for 20 min under vacuum (N816.1.2 KN.45.18/M37, IP20, 0.5 bar, KNF Neuberger, Germany). Two layers were spun on the glass slide at 1000 rpm for 30 s. While the first layer was entirely cured (100 °C for 1 h) in an oven, the second layer was semi-cured at 65 °C for 15 min on a precision hot plate (PR 5-3T, Harry Gestigkeit, Germany). Subsequently, the CNT pattern on the filter membrane was pressed on the semi-cured PDMS layer, and the sample was cured in an oven at 100 °C for 1 h. Afterward, the membrane was soaked in DI water for 2 min and manually detached leaving the CNT pattern embedded into the silicone surface.

For the insulation layer, a 175 μm thick PET foil was cut to the desired dimensions and left in a 10 wt. % SDS solution for 24 h. The foil was dipped two times in DI water and dried by pressurized air. Another PDMS layer (mixed and degassed as mentioned above) was prepared by spin coating (1000 rpm, 150 s) on the PET foil. The foil was attached to a custom-made fineplacer with the PDMS-coated surface facing the embedded CNT pattern. It was aligned onto the CNT pattern such that only electrode openings and contact pads were not covered with the PDMS layer. After placement, the sample was put into a degassing chamber for 20 min and subsequently cured at 150 °C for 1 h. Finally, the foil was detached and the silicone probes were cut to the desired layout before detaching the samples from the glass surface. The complete fabrication process is illustrated schematically in Fig. 1. Images of the samples were made by a stereomicroscope (Stemi 2000-C, Carl Zeiss, Germany) and a camera (EOS 8000D, Canon, Japan) with a microscope adapter (NY1S, Mecan, Japan). The thickness of the PDMS substrate and passivation were determined with a 3D laser scanning confocal microscope (VK-X250, Keyence, Japan). In order to determine the conductivity of the CNT feedlines, samples were cut perpendicular to the length of the feedlines, and their cross section was imaged in a scanning electron microscope (JSM-6060LV, JEOL, Japan) with an acceleration voltage of 10 kV at a magnification of 120×. The

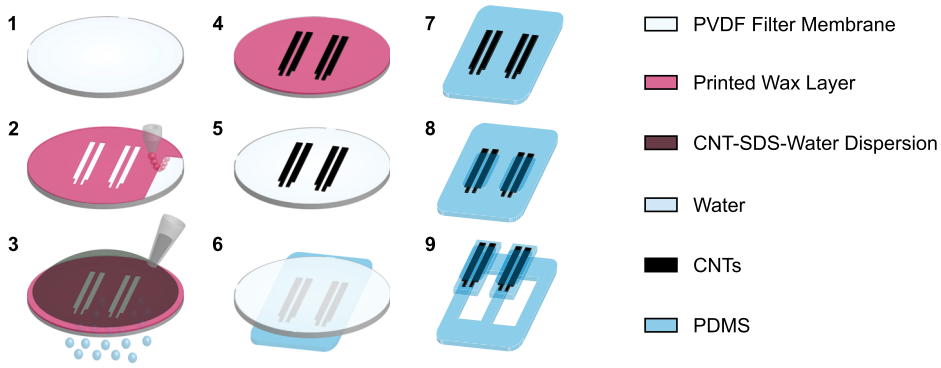

FIG. 1. Fabrication procedure of embedding CNTs into PDMS. A pattern is printed on a blank filter membrane (1 and 2). Vacuum filtration of a CNT-SDS-DI water dispersion through the wax-free areas of the membrane (3). CNTs are deposited on the wax-free areas of the membrane (4), and the wax pattern is dissolved by acetone (5). The CNT pattern is contacted with a semi-cured layer of PDMS (6), and the filter membrane is detached after fully curing the PDMS layer (7). A PDMS top insulation is applied (8), and the samples are cut and detached from the glass carrier (9).

cross-sectional area of the CNT conductors was evaluated with the software Fiji.

For interfacing with the leech, a thread was immersed in PDMS (mixed and degassed as mentioned above) and glued onto the back side of the CNT/PDMS electrodes along the CNT feedlines. The other end of the thread was attached to a surgical needle for suturing.

Electrochemical and mechanical characterization

If not mentioned otherwise, cyclic voltammetry (CV) and impedance spectroscopy measurements were performed in phosphate buffered saline (Dulbecco's PBS, pH = 7, $\rho = 0.63\ \Omega$ m, D8662, Sigma-Aldrich). Both measurements were performed in a three-electrode setup with a Ag/AgCl reference electrode (RE-6, Basi, West Lafayette, USA, 3M NaCl solution), a large-area Pt wire as a counter electrode, and a potentiostat (PalmSens4, The Netherlands). Cyclic voltammetry was applied in three different ranges for different purposes: A scan range between −2.5 V and 2.5 V vs Ag/AgCl for three cycles in order to determine the water oxidation and reduction limits for the CNT/PDMS electrodes and to activate the electrode surface. A scan range between −1 V and 1 V vs Ag/AgCl at 100 mV s^{-1} was applied for ten cycles in order to precondition the surface before performing an electrochemical impedance spectroscopy measurement. A scan range between −0.1 V and 0.1 V vs Ag/AgCl at 10 mV s^{-1} was applied to measure the surface double layer capacitance. The specific capacitance was determined by the formula $c_S = (|i_c| + i_a)/(2 \times |\nu| \times A)$, where i_c and i_a are the cathodic and the anodic current at 0 V vs Ag/AgCl, respectively, ν is the scan rate, and A is the electrode area. In all CVs, the start and finish potential was set to 0 V vs Ag/AgCl, and the measurement started with a negative sweeping direction. The impedance data were recorded applying a signal of 10 mV (rms) (≈28.2 mV peak-to-peak). For comparison, the low-frequency regime of the impedance data (below 20 Hz) was fitted to a simplified Randles circuit neglecting the Warburg element.

In order to determine the charge injection capacity (CIC) and to perform the long-term stimulation experiments, pairs of electrodes on the same electrode array with similar surface area and impedance were characterized. A self-made constant-current source was used to apply stimulation pulses, and the polarization of both electrodes was measured with an oscilloscope (InfiniiVision DSOX2024A, 200 MHz, 2 GSa/s, Keysight, USA). A biphasic (cathodic first), charge-balanced current pulse of 200 μs phase duration and 20 μs interphase delay was applied between both electrodes. The amplitude of the signal was increased until the polarization of each electrode reached $\Delta\varphi_p \approx 1$ V. The polarization was obtained by the formula $\Delta\varphi_p = (\Delta\varphi_{tot} - \Delta\varphi_s)/2$, where $\Delta\varphi_{tot}$ is the total measured potential difference before and at the end of the cathodic pulse and $\Delta\varphi_s$ is the voltage drop over the solution resistance. The CIC was determined by the formula $CIC = Q/A$, where Q is the charge passed through both electrodes during one phase and A is given by the average area of the two electrodes.

The long-term stability upon periodic pulsing was determined by applying continuous pulses between each pair of electrodes, which were used to determine the CIC. Using an identical signal as described above, the current amplitude was determined by the mean electrode area of both electrodes and a charge injection limit (CIL) of 32 μC cm^{-2}. The frequency of the pulse train was 200 Hz, and it was applied for one hour a day. Afterward, an impedance spectrum of both electrodes was recorded separately. In total, this measurement was performed twice a week over a period of three weeks.

For the mechanical characterization, samples with a 20 mm long and 0.6 mm wide CNT/PDMS pattern were attached to a custom-made stretcher and stretched between 0% and 20% strain in a cyclic manner. The stretching speed was set to 0.5 mm s^{-1}. Their resistance was measured after 1, 10, 100, and 1000 and after every additional 1000 cycles until 10 000 cycles were completed. Furthermore, a sequence of cycles with increasing maximum strain of 10% for each cycle was applied up to a total strain of 80%. The resistance of the CNT/PDMS structure was measured after each cycle. The mechanical characterization was performed on $n = 6$ electrodes, and the reported values indicate the mean ± standard deviation.

In vivo surgery

Before the experiment, the leeches (Blutegelapotheke Biebertal, Germany) were kept in tap water (chlorine-free), which was obtained by letting the tap water rest for at least 48 h under ambient conditions. They were stored isolated from light and kept in a fridge at 10 °C. Their water was changed once a week by replacing half of the amount with fresh water. Prior to surgery, the leech was anesthetized by submersion into ice water for ~20 min,

rendering them easier to handle. Then, the leech was pinned down on both ends and the middle with its ventral side facing upwards. Throughout the experiment, the leech was wetted several times with the cold Ringer solution (115.3 mM NaCl, 1.8 mM $CaCl_2$, 4.0 mM KCl, 10 mM, Tris/maleic acid or HEPES). A small longitudinal incision centered over the ventral midline of the leech was performed. The skin and the muscle layers were carefully separated until the nerve cord was exposed. Next, the black sheath surrounding the nerve was cut but not separated, leaving the nerve exposed from above.

The surgical needle that was attached to the nerve interface by a thread was inserted between the nerve cord and the surrounding sheath. Afterward, the thread was used to pull the electrode directly below the nerve to form a tight contact. The other end of the nerve interface was connected to a custom-made holder via an FPC connector (2005280040, Molex, USA). A large-area Pt wire, which was immersed in 2 cm–3 cm proximity to the CNT/PDMS electrodes in the Ringer solution, served as the counter electrode.

In vivo experiment

The stimulation was performed using trains of charge-balanced biphasic current pulses (cathodic pulse first) applied between the CNT/PDMS working and the Pt counter electrode. Each phase had a duration of 200 μs, an interphase delay, and an interpulse delay of 75 μs. The pulse trains consisted of an integer multiple of 100 biphasic pulses. The number of pulse trains and the amplitudes were adjusted until a contraction of the leech could be observed. At the same time, the potential difference between the CNT/PDMS stimulation electrodes and the Pt counter was measured via an oscilloscope, as described for the electrode characterization. During the amplitude adjustment, attention was given not to exceed the water window of the CNT/PDMS electrodes.

RESULTS AND DISCUSSION

An example of a fabricated freestanding CNT/PDMS nerve interface can be seen in Fig. 2(a). The PDMS substrate and passivation thickness are 188 ± 10 μm and 41 ± 13 μm, respectively. The stimulation electrodes have a surface area of 0.16 ± 0.03 mm^2. The CNT feedlines have a cross-sectional area of (4.9 ± 0.7) × 10^4 μm^2 and a thickness of 77 ± 13 μm. The conductivity of the CNT feedlines is 262 ± 35 S m^{-1} directly after fabrication and decreases to 173 ± 27 S m^{-1} after release from the glass carrier. We attribute this difference to the uniaxial strain to which the sample is exposed during release. In Fig. 2(b), the resistance change after stretching the feedline with 20% strain up to 10 000 cycles is shown. During the first ten cycles, we observe an increase of the feedline resistance in the range of ≈5%, followed by a decrease (≈−15% of the original value) after a few thousand cycles. Afterward, the resistance remains stable. Applying increased strains up to 80% leads to an approximately twofold increase in the feedline resistance after relaxation (see Fig. 1 of the supplementary material), which is an acceptable value. The nerve interface is expected to be bent and stretched during normal body movements after being implanted. Therefore, the increase in resistance during the initial stretching cycle of the fabrication procedure can be neglected. These results validate the functionality of the CNTs embedded into PDMS to be used as reliable and stretchable feedlines for implantable nerve interfaces.

From a cyclic voltammetry measurement in the range between −2.5 V and 2.5 V vs Ag/AgCl [Fig. 3(a)], the water oxidation and reduction limits of the CNTs were found to be ~−1.5 V and 1.7 V vs Ag/AgCl by extrapolation of the oxidation and reduction slopes to the voltage axis. This corresponds to a water window that is notably larger than that of the commonly used stimulation electrodes from platinum, which spans approximately a range from −0.6 V to 0.9 V vs saturated calomel electrode (SCE).[5] The reduction and oxidation limits are similar to values reported in the literature for bare CNT fibers.[37]

By performing CV beyond the water window, cathodic and anodic Faradaic currents are generated at the electrodes. As a result, the impedance of the electrodes decreased from 26 ± 4 kΩ to 3.9 ± 0.3 kΩ at 1 kHz [n = 12, mean ± standard deviation; Fig. 4(a)]. Such a decrease was previously observed for carbon nanotube electrodes with an insulating epoxy as the substrate.[39] In our experiments, this decrease was sustained during repetitive measurements in fresh PBS. A possible explanation for this phenomenon is that fabrication-induced contaminations adsorbed at the surface are removed during the CV scan, effectively increasing the accessible surface area. Furthermore, hydrolysis could alter the pH around the electrode, which might induce edge-plane defects or oxygen-containing functional groups on the carbon nanotube surface.[40] Such functional groups can decrease the electrode's impedance by a pseudocapacitive contribution due to redox reactions. SEM images of the CNT surface before and after activation are shown

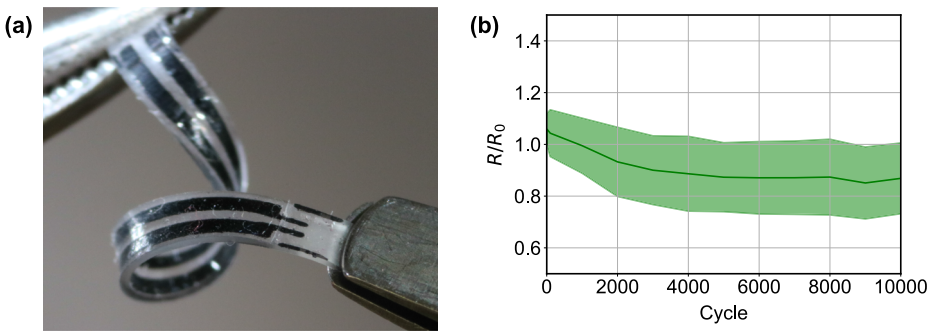

FIG. 2. (a) Image of the freestanding CNT/PDMS nerve interface (scale bar: 3 mm). (b) Resistance change upon cyclic stretching to 20% strain (n = 6, dark green line: mean value, light green area: standard deviation).

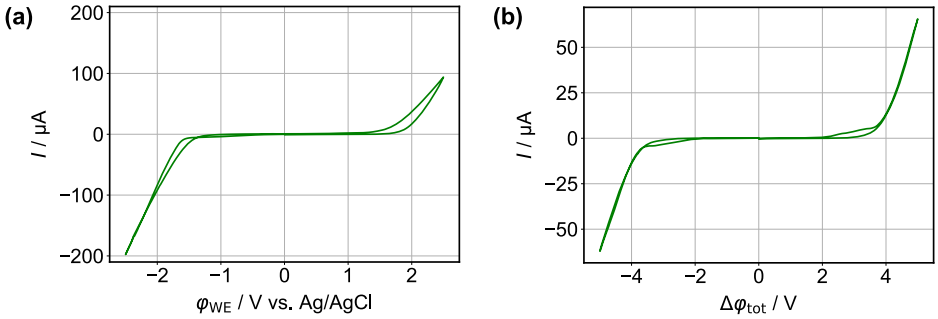

FIG. 3. Cyclic voltammograms used to determine reduction and oxidation limits of water for carbon nanotube electrodes. (a) Measurement on a CNT electrode in a three-electrode-configuration. (b) Measurement between two CNT electrodes on the same electrode array.

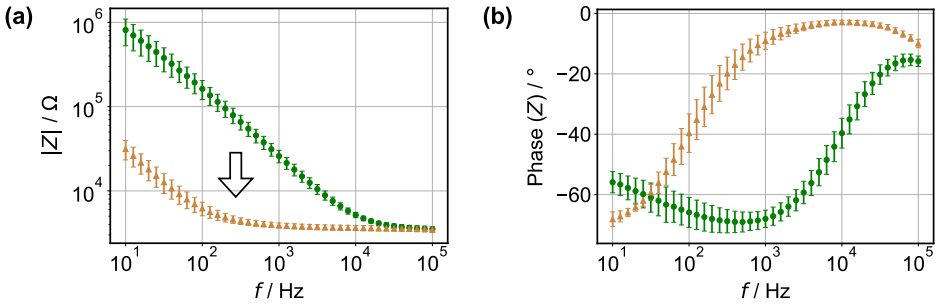

FIG. 4. Impedance spectroscopy of CNT/PDMS electrodes with an area of 0.16 ± 0.03 mm^2 (n = 12, mean ± standard deviation). (a) Change in impedance and (b) change in phase angle before (circles) and after (triangles) surface activation via cyclic voltammetry. The arrows show the direction of change.

in the supplementary material (Fig. 2). Comparing the decreased impedance values with, for example, gold electrodes patterned on PDMS, the areal impedance at 1 kHz is lower (0.6 kΩ mm^2 for CNT/PDMS vs 49.6 kΩ mm^2 [41] and 4.6 kΩ mm^2 [42] for Au on PDMS). However, when the comparison is done with gold electrodes with increased surface roughness by reactive ion etching (0.8 kΩ mm^2 [43] at 1 kHz), the areal impedance values are similar. Platinum-coated titanium oxide nanowire electrodes can show significantly lower impedances.[28] It is noteworthy to mention that the final impedance of our device is strongly affected by the CNT feedline resistance, which is 2.7 ± 0.4 kΩ (n = 12, mean ± standard deviation). Future work should, therefore, be directed at decreasing the feedline resistance, e.g., by changing material properties or geometric design.

The specific capacitance of the CNT/PDMS electrodes was determined from CV measurements (see Fig. 5) to be 0.7 ± 0.2 mF cm^{-2} (n = 12, mean ± standard deviation), which is approximately one order of magnitude less than what was reported for lithographically patterned CNT electrodes.[34,36,44] A possible reason for this might be that the CNTs in this work are partially embedded in PDMS, which decreases the effective surface area of the electrode. It was shown that aligned CNT films possess a larger pore size as well as a more regular pore structure and conductive paths compared to entangled CNTs.[45] Due to the smaller and more irregular pores in entangled CNT electrodes, ions cannot diffuse easily to the inner region of the electrode, ultimately leading to a lower specific electrode capacitance. For comparison, we evaluated the specific capacitance by fitting a simplified Randles circuit to the impedance spectra. In the low-frequency region, where the capacitive contribution dominates, a value of 0.4 ± 0.1 mF cm^{-2} is obtained (n = 12, mean ± standard deviation). However, it should be considered that the interface behavior is not exactly described by the Randles circuit and the results are frequency dependent.

An important property of electrodes used for neural stimulation is the maximum amount of charge that can be injected into the tissue during a stimulation pulse. Associated with this quantity is the so-called charge storage capacity (CSC), which is obtained by integrating the current during a cyclic voltammetry measurement in between the water window of the electrode material. Since only one phase, regardless of whether the stimulation pulse is monophasic or biphasic, is responsible for the generation of an action potential,

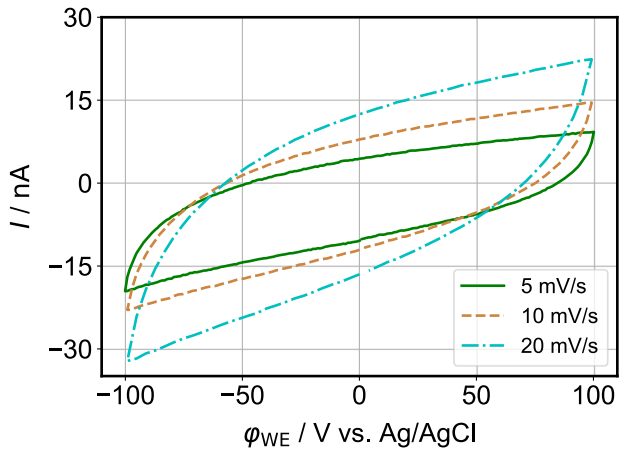

FIG. 5. Cyclic voltammetry performed with a CNT/PDMS electrode (0.143 mm^2) at different scan rates.

only the cathodic or anodic part of the overall charge is considered. However, this assessment method is quasi-stationary (with a duration of up to a few minutes) and does not represent the process of stimulation, which typically relies on short voltage or current pulses (from tens of micro- to a few milliseconds). Another method is to measure the voltage transient at the stimulation electrode vs a reference electrode upon the application of a current pulse. Here, the current amplitude is increased until the electrode polarization (measured as the total potential difference minus the potential drop across the solution resistance) has reached either the water oxidation, water reduction, or any other specified potential. In case the applied signal is a biphasic pulse, the charge in the leading phase is then named as the charge injection limit (CIL) or charge injection capacity (CIC). Since it was shown theoretically and experimentally that cathodic currents provide more efficient stimulation,[46,47] the CIC values reported in the literature are determined mainly using a cathodic leading phase. Important to mention is that the CIC values are in general lower than the CSC values. During CIC assessment, the electrode is at its open circuit potential (somewhere between the water oxidation and reduction potentials) at the onset of the stimulation pulse. Thus, the polarization does not occur across the entire water window as is the case during a CV measurement for the determination of the CSC value. Furthermore, the CIC is not only dependent on the electrode material but also on the duration of the applied stimulation current. Hence, for the determination of the CIC, the exact shape and temporal characteristics of the stimulation pulse should be considered as well.

In this work, the CIC measurement was performed between two electrodes on a single electrode array. After having determined the water window for the CNT/PDMS electrodes, a conservative value of 1 V was set as the target polarization of one electrode and a total polarization of 2 V was used to determine the CIC. Using two similar electrodes on the same stimulation device has the advantage that the measurement can also be performed during *in vivo* experiments. Such an approach is more problematic for the general three-electrode setup due to the possible leakage of potentially harmful materials of the reference electrode into the organism (e.g., silver from a Ag/AgCl reference electrode). An additional CV was carried out across both electrodes to show that the entire system (electrode–electrolyte–electrode) can be operated up to 2 V without significant effects of electrolysis [Fig. 3(b)]. Using this approach, the CIC of the CNT electrodes was calculated to be 81 ± 19 μC cm^{-2} (n = 6 electrode pairs, mean ± standard deviation).

In order to assess the long-term electrochemical stability, we exposed the CNT/PDMS electrodes to >4 × 10^6 stimulation pulses over a time period of three weeks. As during the characterization, the pulses were applied between two CNT/PDMS electrodes and the polarization was evaluated. The charge density was set to 32 μC cm^{-2} per phase, which is close to the allowed upper limit for deep brain stimulators (30 μC cm^{-2}) and for cochlear implants to be used in patients.[48–50] Despite the applied 4 × 10^6 stimulation pulses, no severe change was found in the electrode properties, such as polarization [Fig. 6(a)] or electrode impedance [Fig. 6(b)]. This shows that the CNT/PDMS electrodes are capable of withstanding prolonged stimulation conditions.

The functionality of the electrodes to provide successful stimulation was validated by stimulating the central nerve cord of a horse leech between two randomly selected ganglia [Figs. 7(a) and 7(b)]. In order to prevent electrode potential drift and irreversible damage due to unidirectional Faradaic currents, a biphasic current pulse was chosen. A contraction along the entire leech body was evident when stimulating with a pulse train of 1000 pulses. The stimulation threshold was determined by increasing the stimulation amplitude, and the initial contractions could be observed for a stimulation current of 245 μA (35.0 μC cm^{-2} per phase). Increasing the current to 305 μA (43.6 μC cm^{-2} per phase), the contraction was clearly visible under these conditions. To assess the dependency of stimulation on the number of applied pulses, we decreased the total pulse number in steps of 100 pulses. For this experiment, a stimulation amplitude of 619 μA (88.4 μC cm^{-2}) was applied to ensure reliable stimulation conditions, well above the threshold. Below a pulse number of 300, the leech did not respond to the stimulation conditions. Therefore, the lower thresholds for further experiments were determined to be either a pulse train of 1000 pulses with an amplitude of 305 μA or a pulse train of 400 pulses with an amplitude of 619 μA. Noteworthy is that when increasing the delivered charge during a pulse train, there was no difference in contraction intensity, which indicates that the contraction is due to elicited action potentials in the target nerve area. Next, the minimum time between two stimulation trains for a successful stimulation event was investigated. For this, an amplitude of 619 μA and a pulse number of 800 pulses were applied in order to avoid operation at the stimulation threshold. Thus, a contraction can be ensured given that there is enough time in between two

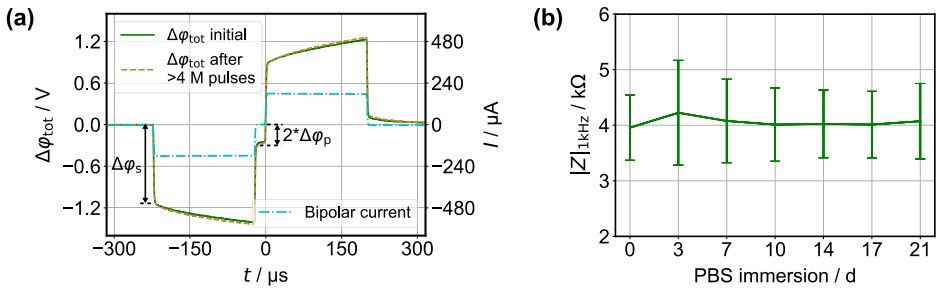

FIG. 6. (a) Voltage transient at an exemplary interface (CNT/PDMS electrode–PBS–CNT/PDMS electrode) upon application of a biphasic constant-current pulse. The current amplitude was set to have a charge density of 32 μC cm^{-2} per phase. (b) Change in electrode impedance upon leaving the electrodes immersed in PBS and having applied one hour of continuous stimulation per day for six days over three weeks (n = 12, error bars show the standard deviation).

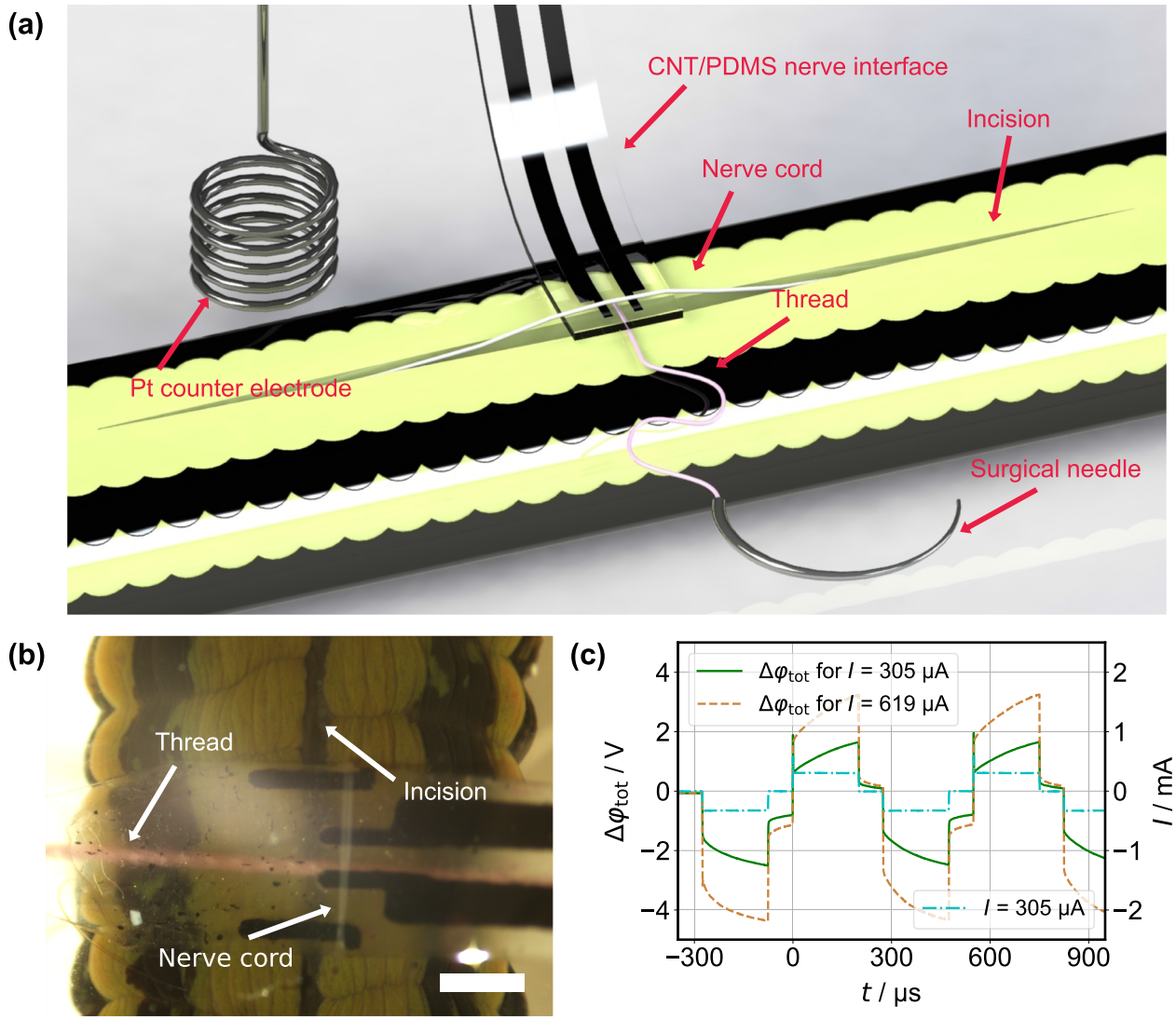

FIG. 7. (a) Schematic of the surgical and experimental setup. (b) CNT/PDMS electrodes interfacing the main nerve cord of the horse leech (scale bar: 1 mm). Only one CNT electrode (upper one) was used for stimulation (A = 0.14 mm^2). (c) Electrode polarization upon passing constant currents with two different amplitudes.

consecutive stimulations. The duration in between two consecutive pulse trains was decreased from 11 s to 1 s. For stimulation frequencies below 0.5 Hz (2 s delay between pulse trains), the subsequent contractions following the first one visibly decreased in strength. These durations are much longer than the refractory period of an axonal action potential, which is in the order of a few milliseconds. Thus, we attribute this outcome to the sluggish relaxation of the contracting muscles, which cannot follow the stimulation repetitions. We characterized the potential excursion of the interface CNT/PDMS electrode–nerve/ringer solution–Pt wire during the stimulation of the leech. The polarization reaches up to 1.05 V for the amplitude of 305 μA and up to 1.5 V for the amplitude of 619 μA [Fig. 7(c)]. In this scenario, the Pt counter electrode has a large area (≈44 mm^2), and thus, its contribution to the overall polarization should be very small or negligible. Therefore, the CNT/PDMS electrodes used in this study were able to successfully elicit action potentials while staying within their water window.

CONCLUSION

In this work, we have fabricated and investigated a stretchable CNT/PDMS electrode for peripheral nerve stimulation. The fabrication relies on wax printing and vacuum filtration to pattern CNT conductive feedlines and electrodes embedded into the surface of PDMS. We investigated the response of the CNT/PDMS

electrodes to repetitive uniaxial stretching (10 000 cycles) and continuous application of stimulation pulses (>4 × 10^6) to which they resisted without failure indicated by the feedline resistance or electrode impedance. The functionality of the CNT/PDMS electrodes was demonstrated by stimulating the main nerve cord of a horse leech and correlating applied stimuli to the observed muscle contractions along its entire body. This shows that the CNT/PDMS composite can potentially be used as an electrode and feedline material in future implantable nerve interfaces. In order to build a reliable interface between the peripheral nervous system and such a device, a mechanically and electrically stable contact should be established between the target nerve and the electrode area. This might be realized by a cuffing mechanism designed around the electrode area or incorporating tissue bonding strategies with the PDMS substrate.

SUPPLEMENTARY MATERIAL

The results of stretching experiments up to 80% strain and SEM images of activated and non-activated CNT electrodes are available in the supplementary material.

DATA AVAILABILITY

The data that support the findings of this study are available from the corresponding author upon reasonable request.

REFERENCES

[1]R. Molina, M. S. Okun, J. B. Shute, E. Opri, P. J. Rossi, D. Martinez-Ramirez, K. D. Foote, and A. Gündüz, "Report of a patient undergoing chronic responsive deep brain stimulation for Tourette syndrome: Proof of concept," J. Neurosurg. **129**, 308–314 (2018).

[2]A. H. Müller, R. Hagen, C. Pototschnig, G. Förster, W. Grossmann, K. Baumbusch, M. Gugatschka, and T. Nawka, "Laryngeal pacing for bilateral vocal fold paralysis: Voice and respiratory aspects," Laryngoscope **127**, 1838–1844 (2017).

[3]Y. Jimbo, H. P. C. Robinson, and A. Kawana, "Strengthening of synchronized activity by tetanic stimulation in cortical cultures: Application of planar electrode arrays," IEEE Trans. Biomed. Eng. **45**, 1297–1304 (1998).

[4]T. L. Babb and W. Kupfer, "Phagocytic and metabolic reactions to chronically implanted metal brain electrodes," Exp. Neurol. **86**, 171–182 (1984).

[5]T. L. Rose and L. S. Robblee, "Electrical stimulation with Pt electrodes. VIII. Electrochemically safe charge injection limits with 0.2 ms pulses," IEEE Trans. Biomed. Eng. **37**, 1118–1120 (1990).

[6]L. S. Robblee, J. L. Lefko, and S. B. Brummer, "Activated Ir: An electrode suitable for reversible charge injection in saline solution," J. Electrochem. Soc. **130**, 731 (1983).

[7]D. Bogdanski, M. Köller, D. Müller, G. Muhr, M. Bram, H. P. Buchkremer, D. Stöver, J. Choi, and M. Epple, "Easy assessment of the biocompatibility of Ni–Ti alloys by *in vitro* cell culture experiments on a functionally graded Ni–NiTi–Ti material," Biomaterials **23**, 4549–4555 (2002).

[8]C. Böhler, F. Oberüber, T. Stieglitz, and M. Asplund, "Nanostructured platinum as an electrochemically and mechanically stable electrode coating," in *Proceedings of the 39th Annual International Conference of the IEEE Engineering in Medicine and Biology Society* (IEEE, 2017), pp. 1058–1061.

[9]J. D. Weiland and D. J. Anderson, "Chronic neural stimulation with thin-film, iridium oxide electrodes," IEEE Trans. Biomed. Eng. **47**, 911–918 (2000).

[10]X. Luo, C. L. Weaver, D. D. Zhou, R. Greenberg, and X. T. Cui, "Highly stable carbon nanotube doped poly(3,4-ethylenedioxythiophene) for chronic neural stimulation," Biomaterials **32**, 5551–5557 (2011).

[11]D. R. Merrill, M. Bikson, and J. G. R. Jefferys, "Electrical stimulation of excitable tissue: Design of efficacious and safe protocols," J. Neurosci. Methods **141**, 171–198 (2005).

[12]S. F. Cogan, "Neural stimulation and recording electrodes," Annu. Rev. Biomed. Eng. **10**, 275–309 (2008).

[13]R. L. White and T. J. Gross, "An evaluation of the resistance to electrolysis of metals for use in biostimulation microprobes," IEEE Trans. Biomed. Eng. **BME-21**, 487–490 (1974).

[14]L. S. Robblee, J. McHardy, W. F. Agnew, and L. A. Bullara, "Electrical stimulation with Pt electrodes. VII. Dissolution of Pt electrodes during electrical stimulation of the cat cerebral cortex," J. Neurosci. Methods **9**, 301–308 (1983).

[15]W. F. Agnew, T. G. H. Yuen, R. H. Pudenz, and L. A. Bullara, "Neuropathological effects of intracerebral platinum salt injections," J. Neuropathol. Exp. Neurol. **36**, 533–546 (1977).

[16]D. Khodagholy, J. N. Gelinas, T. Thesen, W. Doyle, O. Devinsky, G. G. Malliaras, and G. Buzsáki, "NeuroGrid: Recording action potentials from the surface of the brain," Nat. Neurosci. **18**, 310–315 (2015).

[17]S. P. Lacour, G. Courtine, and J. Guck, "Materials and technologies for soft implantable neuroprostheses," Nat. Rev. Mater. **1**, 16063 (2016).

[18]T. Boretius, J. Badia, A. Pascual-Font, M. Schuettler, X. Navarro, K. Yoshida, and T. Stieglitz, "A transverse intrafascicular multichannel electrode (TIME) to interface with the peripheral nerve," Biosens. Bioelectron. **26**, 62–69 (2010).

[19]N. Xue, T. Sun, W. M. Tsang, I. Delgado-Martinez, S.-H. Lee, S. Sheshadri, Z. Xiang, S. Merugu, Y. Gu, S.-C. Yen, and N. V. Thakor, "Polymeric C-shaped cuff electrode for recording of peripheral nerve signal," Sens. Actuators, B **210**, 640–648 (2015).

[20]D. Khodagholy, T. Doublet, P. Quilichini, M. Gurfinkel, P. Leleux, A. Ghestem, E. Ismailova, T. Hervé, S. Sanaur, C. Bernard, and G. G. Malliaras, "*In vivo* recordings of brain activity using organic transistors," Nat. Commun. **4**, 1575 (2013).

[21]A. Srinivasan, J. Tipton, M. Tahilramani, A. Kharbouch, E. Gaupp, C. Song, P. Venkataraman, J. Falcone, S. P. Lacour, G. B. Stanley, A. W. English, and R. V. Bellamkonda, "A regenerative microchannel device for recording multiple single-unit action potentials in awake, ambulatory animals," Eur. J. Neurosci. **43**, 474–485 (2016).

[22]I. R. Minev, P. Musienko, A. Hirsch, Q. Barraud, N. Wenger, E. M. Moraud, J. Gandar, M. Capogrosso, T. Milekovic, L. Asboth, R. F. Torres, N. Vachicouras, Q. Liu, N. Pavlova, S. Duis, A. Larmagnac, J. Vörös, S. Micera, Z. Suo, G. Courtine, and S. P. Lacour, "Electronic dura mater for long-term multimodal neural interfaces," Science **347**, 159–163 (2015).

[23]F. Decataldo, T. Cramer, D. Martelli, I. Gualandi, W. S. Korim, S. T. Yao, M. Tessarolo, M. Murgia, E. Scavetta, R. Amici, and B. Fraboni, "Stretchable low impedance electrodes for bioelectronic recording from small peripheral nerves," Sci. Rep. **9**, 10598 (2019).

[24]N. Adly, S. Weidlich, S. Seyock, F. Brings, A. Yakushenko, A. Offenhäuser, and B. Wolfrum, "Printed microelectrode arrays on soft materials: From PDMS to hydrogels," npj Flexible Electron. **2**, 15 (2018).

[25]D. S. Gray, J. Tien, and C. S. Chen, "High-conductivity elastomeric electronics," Adv. Mater. **16**, 393–397 (2004).

[26]L. Guo, M. Ma, N. Zhang, R. Langer, and D. G. Anderson, "Stretchable polymeric multielectrode array for conformal neural interfacing," Adv. Mater. **26**, 1427–1433 (2014).

[27]S. P. Lacour, D. Chan, S. Wagner, T. Li, and Z. Suo, "Mechanisms of reversible stretchability of thin metal films on elastomeric substrates," Appl. Phys. Lett. **88**, 204103 (2006).

[28]K. Tybrandt, D. Khodagholy, B. Dielacher, F. Stauffer, A. F. Renz, G. Buzsaki, and J. Vörös, "High-density stretchable electrode grids for chronic neural recording," Adv. Mater. **30**, e1706520 (2018).

[29]J. H. Kim, J. Y. Hwang, H. R. Hwang, H. S. Kim, J. H. Lee, J. W. Seo, U. S. Shin, and S. H. Lee, "Simple and cost-effective method of highly conductive and elastic carbon nanotube/polydimethylsiloxane composite for wearable electronics," Sci. Rep. **8**, 1375 (2018).

[30]Y. Hanein, "Carbon nanotube integration into MEMS devices," Phys. Status Solidi B **247**, 2635–2640 (2010).

[31] B. Luo, Y. Wei, H. Chen, Z. Zhu, P. Fan, X. Xu, and B. Xie, "Printing carbon nanotube-embedded silicone elastomers via direct writing," ACS Appl. Mater. Interfaces **10**, 44796–44802 (2018).
[32] B. Nie, X. Li, J. Shao, X. Li, H. Tian, D. Wang, Q. Zhang, and B. Lu, "Flexible and transparent strain sensors with embedded multiwalled carbon nanotubes meshes," ACS Appl. Mater. Interfaces **9**, 40681–40689 (2017).
[33] C. Lim, D.-H. Min, and S.-B. Lee, "Direct patterning of carbon nanotube network devices by selective vacuum filtration," Appl. Phys. Lett. **91**, 243117 (2007).
[34] T. Gabay, M. Ben-David, I. Kalifa, R. Sorkin, Z. e. R. Abrams, E. Ben-Jacob, and Y. Hanein, "Electro-chemical and biological properties of carbon nanotube based multi-electrode arrays," Nanotechnology **18**, 035201 (2007).
[35] L. Bareket-Keren and Y. Hanein, "Carbon nanotube-based multi electrode arrays for neuronal interfacing: Progress and prospects," Front. Neural Circuits **6**, 122 (2012).
[36] K. Wang, H. A. Fishman, H. Dai, and J. S. Harris, "Neural stimulation with a carbon nanotube microelectrode array," Nano Lett. **6**, 2043–2048 (2006).
[37] F. Vitale, S. R. Summerson, B. Aazhang, C. Kemere, and M. Pasquali, "Neural stimulation and recording with bidirectional, soft carbon nanotube fiber microelectrodes," ACS Nano **9**, 4465–4474 (2015).
[38] K. Tybrandt and J. Vörös, "Fast and efficient fabrication of intrinsically stretchable multilayer circuit boards by wax pattern assisted filtration," Small **12**, 180–184 (2016).
[39] S.-R. Yeh, Y.-C. Chen, H.-C. Su, T.-R. Yew, H.-H. Kao, Y.-T. Lee, T.-A. Liu, H. Chen, Y.-C. Chang, P. Chang, and H. Chen, "Interfacing neurons both extracellularly and intracellularly using carbon–nanotube probes with long-term endurance," Langmuir **25**, 7718–7724 (2009).
[40] C.-C. Hu, J.-H. Su, and T.-C. Wen, "Modification of multi-walled carbon nanotubes for electric double-layer capacitors: Tube opening and surface functionalization," J. Phys. Chem. Solids **68**, 2353–2362 (2007).
[41] I. R. Minev, D. J. Chew, E. Delivopoulos, J. W. Fawcett, and S. P. Lacour, "Evaluation of an elastomer based gold microelectrode array for neuronal recording applications," in *Proceedings of the 5th International IEEE/EMBS Conference on Neural Engineering* (IEEE, 2011), pp. 482–485.
[42] L. Guo, G. S. Guvanasen, X. Lui, C. Tuthill, T. R. Nichols, and S. P. DeWeerth, "A PDMS-based integrated stretchable microelectrode array (isMEA) for neural and muscular surface interfacing," IEEE Trans. Biomed. Circuits Syst. **7**, 1–10 (2013).
[43] E. Delivopoulos, D. J. Chew, I. R. Minev, J. W. Fawcett, and S. P. Lacour, "Concurrent recordings of bladder afferents from multiple nerves using a microfabricated PDMS microchannel electrode array," Lab Chip **12**, 2540–2551 (2012).
[44] M. David-Pur, L. Bareket-Keren, G. Beit-Yaakov, D. Raz-Prag, and Y. Hanein, "All-carbon-nanotube flexible multi-electrode array for neuronal recording and stimulation," Biomed. Microdevices **16**, 43–53 (2014).
[45] H. Zhang, G. Cao, Y. Yang, and Z. Gu, "Comparison between electrochemical properties of aligned carbon nanotube array and entangled carbon nanotube electrodes," J. Electrochem. Soc. **155**, K19 (2008).
[46] F. Rattay, "Analysis of models for extracellular fiber stimulation," IEEE Trans. Biomed. Eng. **36**, 676–682 (1989).
[47] M. B. Voigt and A. Kral, "Cathodic-leading pulses are more effective than anodic-leading pulses in intracortical microstimulation of the auditory cortex," J. Neural Eng. **16**, 036002 (2019).
[48] R. K. Shepherd, G. M. Clark, and R. C. Black, "Chronic electrical stimulation of the auditory nerve in cats. Physiological and histopathological results," Acta Oto-Laryngol. **95**, 19–31 (1983).
[49] S. F. Cogan, K. A. Ludwig, C. G. Welle, and P. Takmakov, "Tissue damage thresholds during therapeutic electrical stimulation," J. Neural Eng. **13**, 021001 (2016).
[50] G. M. Clark, "The multiple-channel cochlear implant: The interface between sound and the central nervous system for hearing, speech, and language in deaf people–a personal perspective," Philos. Trans. R. Soc., B **361**, 791–810 (2006).